

## Radio Frequency Seeker Modelling and Seeker Filter Design

Prashant Vora, P.K. Tiwari, and R.N. Bhattacharjee  
*Defence Research & Development Laboratory, Hyderabad-500 058*

and

Abhijit Bhattacharyya and M. Jyothi  
*Research Centre Imarat, Hyderabad -500 058*

### ABSTRACT

Radio frequency seeker model, including receiver angle error noise modelling and filtering of noise from seeker measurement, is presented in this paper. The effects of eclipsing, radar cross section fluctuation, etc on seeker sight-line rate measurement are highlighted. The formulation for colour noise modelling of sight-line rate noise is derived based on the knowledge of seeker receiver angle error noise model. Two Kalman filter configurations for filtering of noise from seeker output have been considered in this paper, based on sight-line rate kinematics and noise characteristic. It has been observed from the simulation studies that sight-line rate signal varies slowly at higher interceptor-target ranges; with severe colour noise in sight line rate measurement, and therefore higher weightage for noise attenuation is beneficial in Kalman filter configuration. So, kinematic plus state augmentation for colour noise are considered for adequate filtering for higher interceptor-target ranges. Whereas for lower interceptor-target ranges, sight-line rate changes appreciably, which have been tracked by a simplified/modified spherical coordinate model, which uses knowledge of interceptor-target engagement dynamics. For both the filters, benefits of colour noise modelling and process model augmentation through coloured noise states, for filtering severe colour noise of seeker, has been demonstrated.

**Keywords:** RF seeker models, seeker filters, sight-line rate, seeker models, seeker modelling filter design, colour noise modelling, radio frequency seeker model

### NOMENCLATURE

$\theta_{ky}, \theta_{kz}$	Kinematic gimbal angle	$R_{MT}$	Interceptor-target range
$\theta_{my}, \theta_{mz}$	Measured gimbal angle	$V_{MT}$	Interceptor-target closing velocity
$\dot{\theta}_{my}, \dot{\theta}_{mz}$	Measured gimbal angle rate	$\delta_y, \delta_z$	Angle error
$\dot{\lambda}_{KY}, \dot{\lambda}_{KZ}$	Kinematic sight-line rate	$\delta_{YM}$	Measured angle error
$\dot{\lambda}_{MY}, \dot{\lambda}_{MZ}$	Measured sight-line rate	$\sigma_R$	Receiver angle error noise standard deviation
		$S, DY, DZ$	Sum and difference signal of antenna
		$P_{pic}$	Transmitter peak power

Received 15 November 2004

$G$	Antenna gain
$\lambda$	Wavelength
$\sigma$	Radar cross-section fluctuation
$\sigma_{av}$	Mean radar cross-section value
$L_3$	Summed loss
$T_p$	Transmitter pulse repetition period
$\tau_R$	Received pulse duration in receiver gate
$\tau_D$	Delay time
$c$	Speed of light
$\tau$	Correlation interval
$B_c$	Spectral bandwidth at half power level
$K$	Boltzman constant
$T_0$	Environment temperature
$B_R$	Receiver bandwidth
$F_R$	Noise figure of receiver
$\theta_A$	Antenna beam width
$ATL$	Track loop gain
$A_{TY}$	Target acceleration in line-of-sight Y-axis
$A_{MY}$	Interceptor acceleration in line-of-sight Y-axis
$v(t)$	Zero mean white noise
$Q$	Process noise covariance

**1. INTRODUCTION**

Many surface-to-air and air-to-air interceptors use proportional navigation as guidance strategy. Handover errors accumulated at the beginning of terminal phase of guidance due to errors in radar data need to be corrected to achieve low miss-distance. Thus, in terminal phase of guidance, more accurate guidance signal (mainly sight-line rate) is required. The RF seeker is one of the sensor, which can provide accurate guidance signal. However, sight-line rate provided by the RF seeker has time-varying noise statistics of high magnitude, and therefore, a simple digital filter is inadequate to filter the noisy sight-line rate. Moreover, lag of the filter is

to be low for satisfactory guidance performance. To filter the noisy sight-line rate output of seeker, its noise characterisation is important and to characterise receiver angle error noise, basic understanding of seeker model is essential. This paper gives the RF seeker noise model and highlights how various effects like eclipsing, target radar cross-section fluctuations, etc affect the receiver angle error noise, making receiver angle error noise characteristic fully coloured. This, in turn, affects the sight-line rate output from the seeker, having severe coloured noise contamination in signals.

The filtering of colour noise is a challenging problem. One approach of colour noise filtering is to model the colour noises and augment with process model of Kalman filter. Not much literature is available on RF seeker colour noise modelling. This study explores the possibility of colour noise modelling. In this study, formulations for colour noise model have been derived based on seeker receiver noise model. Two different linear Kalman filter configurations augmented with the above coloured noise states of seeker have been designed for filtering of line-of-sight (LOS) rates and their results are compared.

**2. TYPICAL RF SEEKER MATHEMATICAL MODEL**

The functional diagram of a typical RF seeker is shown in Fig. 1 in a simplified form, which is of interest for guidance and filter design. A RF seeker, which uses mono-pulse receiver, is considered.

Input to the antenna model is boresight errors which is the difference between the kinematic gimbal

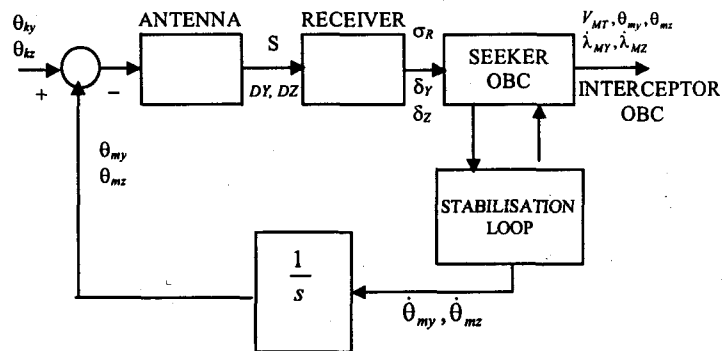


Figure 1. Functional diagram of radio frequency seeker

angles  $\theta_{ky}$ ,  $\theta_{kz}$ , and the measured gimbal angles  $\theta_{my}$ ,  $\theta_{mz}$ . Kinematic gimbal angles and measured gimbal angles are defined in *Appendix A*. Antenna model gives sum and difference channel signals as the function of boresight errors based on the sum and difference antenna patterns, which can be obtained experimentally. Sum and difference signals are input to the receiver block. In this study, for simplicity, it has been assumed that the difference signal is equal to the individual boresight errors, which are directly passed to the receiver model. Receiver block calculates angle errors based on the sum and difference signals and it is passed to the digital signal processing (DSP) block. The angle errors accumulation and averaging operations are done in DSP block, which is part of seeker onboard computer. The seeker onboard computer gives command to antenna stabilisation system, which drives antenna in the direction of the target. The seeker onboard computer does different processing and gives information on line-of-sight rate, gimbal angles, and closing velocity between the interceptor and the target to interceptor onboard computer for guidance at a specific update rate. The seeker onboard computer also gives quality of seeker measurement in terms of angle error variance and signal-to-noise in terms of log detector output, which can be used for seeker filtering.

### 3. RECEIVER NOISE MODEL

The receiver angle error noise can be modelled as a function of signal-to-noise (ie, ratio of antennal sum channel signal and receiver thermal noise)<sup>1</sup>. How the various effects like eclipsing, radar cross-section fluctuation, etc affect the antenna sum power signal, and which in turn affects the angle error through signal-to-noise, are declared.

#### 3.1 Antenna Sum Channel Signal Power Calculation

The signal power,  $S$  received in a sum channel of an antenna<sup>2</sup> is

$$S = \frac{P_{pic} \times G^2 \times \lambda^2 \times \sigma \times L_3}{(4\pi)^3 \times R_{MT}^4} \times \frac{\tau_R^2(R_{MT})}{T_P^2(F_d)} \quad (1)$$

According to Eqn (1), received signal power,  $S$  increases as interceptor-target range decreases. However, because of eclipsing effect and radar cross-section fluctuation, signal power is modulated significantly and attains low values even at lower interceptor-target ranges.

#### 3.1.1 Eclipsing Effect

In a pulsed radar, the target return can arrive when the transmitter is on and the receiver is off. This effect is called the eclipsing effect and it is periodical. The received pulses may be partially or completely eclipsed depending on their relative arrival time wrt the transmitted pulses. The time of target return at the receiver (pulse delay time  $\tau_D$  of a received pulse from a target) depends on the distance between the interceptor and the target. It varies between pulse interval  $0-T_p$ . Delay time  $\tau_D$  can be calculated as follows:

$$\tau_D = T_p \times \text{frac} \left( \frac{2R_{MT}}{cT_p} \right) \quad (2)$$

Assuming transmitter pulse duration  $\tau_T = \frac{T_p}{3}$  and receiver gate duration  $\tau_G = \frac{T_p}{2}$ , pulse duration change of a target pulse past the receiver gate  $\tau_R$ , is calculated by the formula:

$$\tau_R = \begin{cases} 0 & \tau_D < \tau_G - \tau_T \text{ Blind zone} \\ \tau_D + \tau_T - \tau_G & \tau_G - \tau_T \leq \tau_D < \tau_G \text{ Partial zone} \\ \tau_T & \tau_G \leq \tau_D < 2\tau_G - \tau_T \text{ Transparent zone} \\ 2\tau_G - \tau_D & 2\tau_G - \tau_T \leq \tau_D < 2\tau_G \text{ Partial zone} \end{cases} \quad (3)$$

A graphical representation of these equations are shown in Fig. 2.

Based on Eqn (3), eclipsing cycle (ie duration of blind, transparent, and partial received pulses) can be calculated for a particular closing velocity between the interceptor and the target. Blind zone is calculated as follows:

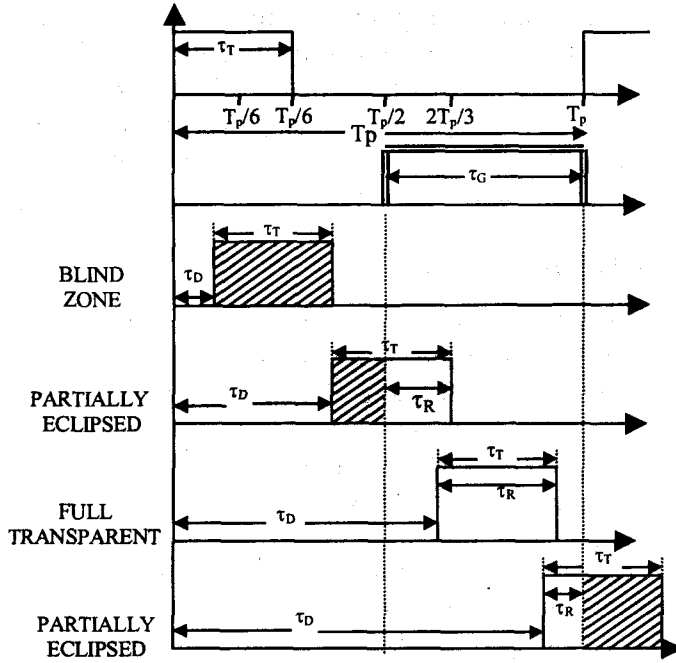


Figure 2. Eclipsing effect

$$\tau_{d1} - \tau_{d2} = \frac{T_p}{6} = T_p * \left( \text{frac} \left( \frac{2 * V_{MT} * t2}{c * T_p} \right) - \text{frac} \left( \frac{2 * V_{MT} * t1}{c * T_p} \right) \right)$$

For same integer part of real number:

$$\frac{T_p}{6} = T_p * \left( \frac{2 * V_{MT} * (t2 - t1)}{c * T_p} \right) \Rightarrow t_{blind} = \frac{c * \left( \frac{T_p}{6} \right)}{2 * V_{MT}}$$

Similarly, transparent and partial eclipsing zones can be written as

$$t_{transparent} = \frac{c * \left( \frac{T_p}{6} \right)}{2 * V_{MT}} \quad t_{partial1} = t_{partial2} = \frac{c * \left( \frac{T_p}{3} \right)}{2 * V_{MT}}$$

So, eclipsing period is:

$$t_{eclipse} = t_{blind} + t_{transparent} + 2t_{partial} = \frac{c * T_p}{2 * V_{MT}}$$

It is clear from the above formula that full signal received duration (ie, transparent period) is

only 16 per cent of the eclipsing period. In other words, it can be said that the eclipsing effect modulates the received signal significantly.

### 3.1.2 Radar Cross-section Fluctuation

The radar cross section is effective cross section of target seen by the radar/seeker. Here, for simulating target RCS fluctuation, swerling case 1 is chosen<sup>3</sup>. The radar cross-section fluctuation is simulated by stochastic process with the exponential distribution law.

$$\rho = e^{(-2\pi B_c \tau)}$$

The exponential process corresponding to radar cross-section fluctuation can be presented as the sum of squares of two identical independent normal stochastic processes with math expectation equal to zero and dispersion  $2\sigma_{av}$ .

or

$$\xi_1(n) = \rho \xi_1(n-1) + N_1(0,1) \sqrt{\frac{(1-\rho^2) \sigma_{av}}{2}}$$

$$\xi_2(n) = \rho \xi_2(n-1) + N_2(0,1) \sqrt{\frac{(1-\rho^2) \sigma_{av}}{2}}$$

The radar cross-section amplitude fluctuation ( $\sigma$ ) is given as

$$\sigma = \xi_1^2 + \xi_2^2 \tag{4}$$

The target radar cross-section fluctuation is low-frequency fluctuation, which also modulates the signal-to-noise ratio (SNR), and thereby the received signal.

### 3.2 SNR & Receiver Angle Error Calculation

Thermal noise power of the receiver is calculated as follows:

$$(N_p) = K \times T_0 \times B_R \times F_R \times \frac{\tau_G}{T_p} \tag{5}$$

So, SNR can be written as

$$\text{SNR} = \frac{\text{Received sum signal power}}{\text{Receiver thermal noise power}}$$

Skolnik<sup>1</sup> has given the relation for receiver angle error noise standard deviation, with antenna beam width; SNR and this is as follows:

$$\sigma_R = \frac{\sqrt{3}\theta_A}{\pi\sqrt{\text{SNR}}} \quad (6)$$

Receiver angle error noise can be generated as zero mean Gaussian noise with standard deviation calculated as above.

For low SNR; tracking error mean measured by seeker is appreciably lower as per the following empirical relation obtained for radio frequency seeker:

$$\delta_Y = \frac{\text{SNR}}{\text{SNR} + 3} DY \quad (7)$$

Thus, for low SNR, mean of angle error is low and  $\sigma_R$  is high.

Receiver angle errors are calculated by adding tracking error mean, which is calculated, based on Eqn (7) to the generated Gaussian noise as a function of SNR. Schematic diagram of simplified receiver model is shown in Fig. 3.

It can be said that angle errors have time-varying noise statistics because of eclipsing effect and radar cross-section fluctuation effect. As described in Section 2, angle errors are passed to the DSP

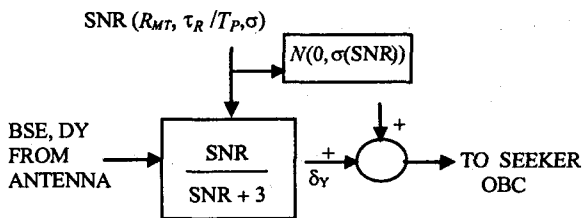


Figure 3. Receiver model

block, which processes the angle errors and generates antenna drive command, which in turn drives the antenna in the direction of the target. Owing to the limited filtering capability of DSP block, good amount of coloured noise along with signal passes to the seeker stabilisation system as commanded dish rate, which is taken as seeker line-of-sight rate measurement for guidance. In addition, these noises are also passed to the antenna stabilisation system, causing antenna to fluctuate at low frequency. This fluctuation directly appears in boresight error, and thus results in additional low-frequency component of noise appearing in seeker measurement. In other words, seeker measurements are coloured in nature.

#### 4. COLOUR NOISE MODELLING & KALMAN FILTER CONFIGURATION

##### 4.1 Colour Noise Modelling

Formulation for colour noise modelling is derived based on the block diagram shown in Fig. 4.

Assuming unity gain for stabilisation loop, measured sight-line rate along the Y-axis in seeker frame (see Appendix A) is written as:

$$\dot{\lambda}_{MY} = (\dot{\lambda}_{KY} - \dot{\lambda}_{MY}) \frac{1}{s} ATL \frac{\text{SNR}}{\text{SNR} + 3} * \frac{1}{1 + T_{DSP}s} + \frac{N(0, \sigma_R(\text{SNR}_{dB}))}{1 + T_{DSP}s} ATL \quad (8)$$

Track loop gain to be selected by guidance designer and DSP block is assumed as first-order TF.

$$\frac{\delta_{YM}}{\delta_Y} \approx \frac{1}{1 + T_{DSP}s}$$

So, measured sight-line rate can be written as a combination of kinematic and noise part of sight-line rate, which takes care eclipsing effect and radar cross-section fluctuations (as  $\sigma_R$  obtained as a function of SNR, which is modulated by eclipsing and radar cross-section fluctuations).

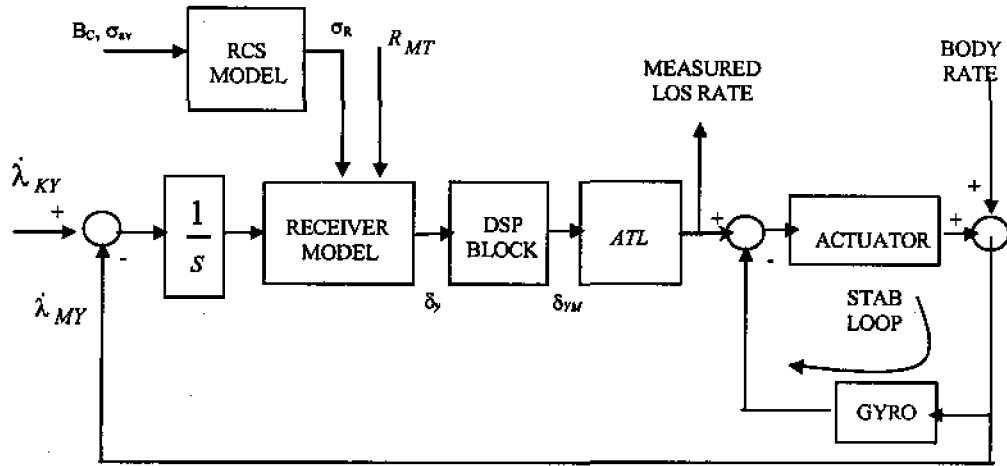


Figure 4. Basic block diagram of seeker tracking and stabilisation system

$$\dot{\lambda}_{MY} = \frac{\dot{\lambda}_{KY}}{\frac{s}{ATL'} + 1} + \frac{N(0, \sigma_R) * ATL}{1 + T_{DSP}s} - \frac{N(0, \sigma_R) * ATL}{\frac{s}{ATL'} + 1} \quad (9)$$

where

$$ATL' = ATL * \frac{SNR}{SNR + 3}$$

Based on the Eqn (9), colour noise states can be derived and augmented to the basic equation of process model of Kalman filter. Here, the simplified noise part of sight-line rate is used to avoid cross correlation between the process noise and the measurement noise.

Assumption for simplification is the factor  $T_{DSP} * ATL' \ll 1$ . With this

$$\dot{\lambda}_{Noise} \approx \frac{N(0, \sigma_R) * ATL}{1 - T_{DSP} * ATL'} \left( \frac{1}{T_{DSP}s + 1} - \frac{1}{\frac{s}{ATL'} + 1} \right) \quad (10)$$

Assuming  $\frac{T_{DSP}}{ATL'} \ll 1$  and substituting Eqn (10) into the Eqn (9), measured sight-line rate can be written as

$$\dot{\lambda}_{MY} = \frac{\dot{\lambda}_{KY}}{\frac{s(1+T_{DS}s)}{ATL} + 1} + \frac{N(0, \sigma_R(SNR_{dB})) * s * ATL}{\left(\frac{s(1+T_{DS}s)}{ATL'} + 1\right) * ATL'} \dot{\lambda}_{KY} + \dot{\lambda}_{Noise}$$

The same formulation can be derived for measured sight-line rate along Z-axis in seeker frame.

#### 4.2 Kalman Filter Configuration

In this work, two Kalman filter configurations have been considered. The process models of both configurations have been augmented with three-colour noise states to take care of varying noise statistics of measurement. In the first Kalman filter configuration, process model is having three states—line-of-sight rate, two higher-order derivatives of line-of-sight rate  $[\dot{\lambda} \ \ddot{\lambda} \ \ddot{\lambda}]$ , and the third state is driven by white noise. While in second Kalman filter configuration, the process model is taken based on modified spherical coordinate model<sup>4</sup>. In this study, modified spherical coordinate model is simplified based on small angle approximation to avoid nonlinearity.

Seeker measurements are available in seeker frame (*Appendix A*). To formulate colour noise state equations in inertial frame, first the measurements are transformed from the seeker frame to the inertial frame (ie line-of-sight frame, *Appendix B*).

$$\begin{bmatrix} \dot{\lambda}_{MY} \\ \dot{\lambda}_{MZ} \end{bmatrix}_{inertial} = \begin{bmatrix} T_{22} & T_{23} \\ T_{31} & T_{32} \end{bmatrix}_{seeker2inertial} \begin{bmatrix} \dot{\lambda}_{MY} \\ \dot{\lambda}_{MZ} \end{bmatrix}_{seeker} \quad (11)$$

So, measured sight-line rate along the inertial Y-axis can be written as

$$\begin{aligned} \dot{\lambda}_{MY\text{inertial}} &= T_{22} * \dot{\lambda}_{MY\text{seeker}} + T_{23} * \dot{\lambda}_{MZ\text{seeker}} \\ &= \frac{T_{22} * \dot{\lambda}_{KY} + T_{23} * \dot{\lambda}_{KZ}}{\frac{s}{ATL'} + 1} + \\ &\quad \frac{N(0, \sigma_R) * ATL(T_{22} + T_{23})}{1 + T_{DSP}s} - \\ &\quad \frac{N(0, \sigma_R) * ATL(T_{22} + T_{23})}{\frac{s}{ATL'} + 1} \quad (12) \\ &= x_1 + x_2 - x_3 \end{aligned}$$

Based on the above equation, colour noise states are derived. To filter sight-line rate along line-of-sight Y-axis, Kalman filter process models and measurement models are as follows:

#### 4.2.1 Process Model 1

The process model, which comprises three kinematic states plus augmentation with noise states is obtained as follows:

$$\frac{d}{dt} \begin{bmatrix} \dot{\lambda}_{KY} \\ \ddot{\lambda}_{KY} \\ \ddot{\lambda}_{KY} \\ x_1 \\ x_2 \\ x_3 \end{bmatrix} = \begin{bmatrix} 0 & 1 & 0 & 0 & 0 & 0 \\ 0 & 0 & 1 & 0 & 0 & 0 \\ 0 & 0 & 0 & 0 & 0 & 0 \\ ATL & 0 & 0 & -ATL' & 0 & 0 \\ 0 & 0 & 0 & 0 & \frac{-1}{T_{DSP}} & 0 \\ 0 & 0 & 0 & 0 & 0 & -ATL' \end{bmatrix} \begin{bmatrix} \dot{\lambda}_{KY} \\ \ddot{\lambda}_{KY} \\ \ddot{\lambda}_{KY} \\ x_1 \\ x_2 \\ x_3 \end{bmatrix} + \begin{bmatrix} 0 \\ 0 \\ w_1 \\ 0 \\ N(0, \sigma_R) * \frac{ATL}{T_{DSP}} * (T_{22} + T_{23}) \\ N(0, \sigma_R) * ATL * ATL' * (T_{22} + T_{23}) \end{bmatrix}$$

#### 4.2.2 Process Model 2

The process model, which comprises simplified MSC model, using known interceptor-target relations plus augmentation with noise states, is obtained as follows:

$$\frac{d}{dt} \begin{bmatrix} \dot{\lambda}_{KY} \\ x_1 \\ x_2 \\ x \end{bmatrix} = \begin{bmatrix} \frac{-2}{tgo} & 0 & 0 & 0 \\ ATL' & -ATL' & 0 & 0 \\ 0 & 0 & \frac{-1}{T_{DSP}} & 0 \\ 0 & 0 & 0 & -ATL' \end{bmatrix} \begin{bmatrix} \dot{\lambda}_{KY} \\ x_1 \\ x_2 \\ x_3 \end{bmatrix} + \begin{bmatrix} w_1 \\ 0 \\ N(0, \sigma_R) * \frac{ATL}{T_{DSP}} * (T_{22} + T_{23}) \\ N(0, \sigma_R) * ATL * ATL' * (T_{22} + T_{23}) \end{bmatrix} + \begin{bmatrix} \frac{A_{TY} - A_{MY}}{R_{MT}} \\ 0 \\ 0 \\ 0 \end{bmatrix}$$

$w_1$  is zero mean white noise and  $N(0, \sigma_R)$  is receiver noise, The target and interceptor accelerations are available from radar and inertial navigation system and transformed to line-of-sight Y-axis.

#### 4.2.3 Measurement Model 1

$$Z = [0 \ 0 \ 0 \ 1 \ 1 \ -1]X + v(t)$$

#### 4.2.4 Measurement Model 2

$$Z = [0 \ 1 \ 1 \ -1]X + v(t)$$

where  $X$  is the state vector for corresponding process models and  $Z$  is the sight-line rate measurement in seeker frame transformed to line-of-sight Y-axis. Similar Kalman filter configurations are used for sight-line rate filtering along line-of-sight Z-axis.

## 5. SIMULATION RESULTS

For simulation, a typical RF seeker is assumed, which is having a tracking range of 10 km for a target radar cross section of 1 m<sup>2</sup>. Hypothetical interceptor and target are considered for the generation of seeker model simulation environment. Figures 5 and 6 show the effect of radar cross-section fluctuation and eclipsing on SNR. It can be seen in both the cases that SNR is fluctuating between normal (ie, without considering eclipsing effect and radar cross-section fluctuation) to lower value, while in normal case, increases as interceptor-target

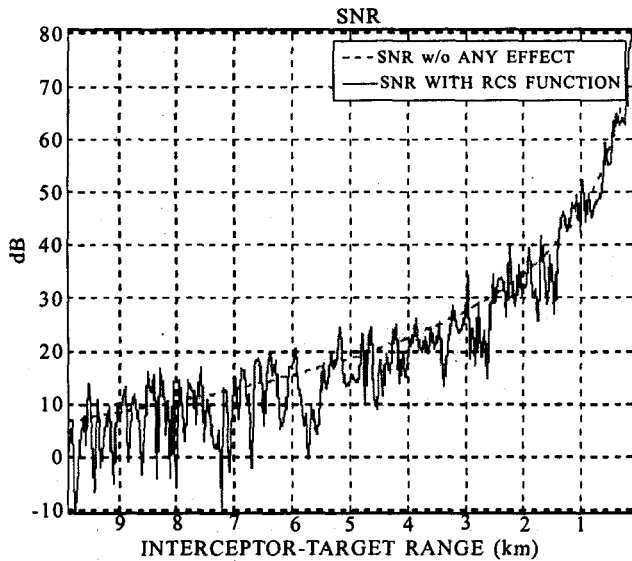


Figure 5. SNR with radar cross-section fluctuation

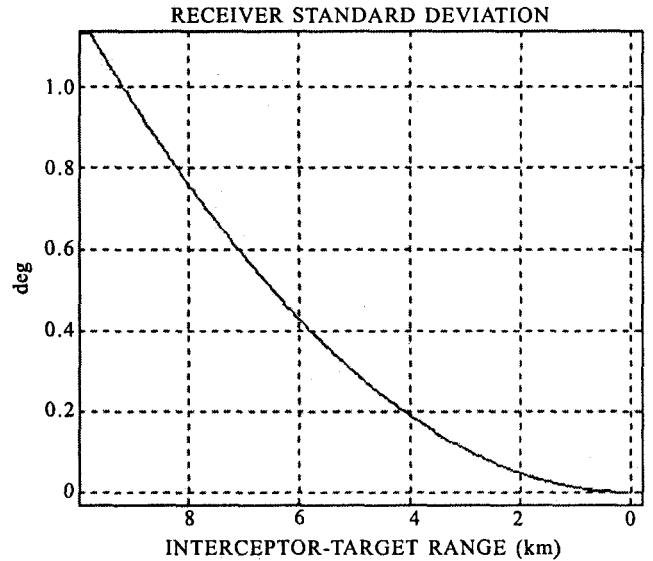


Figure 7. Receiver noise standard deviation without radar cross-section fluctuation and eclipsing effect.

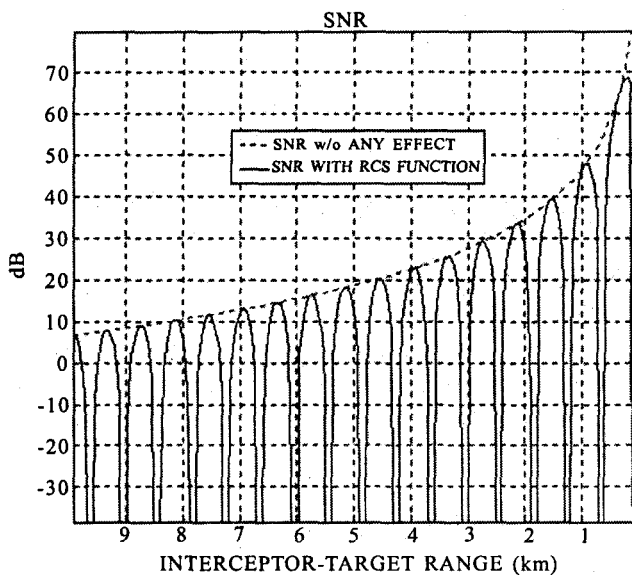


Figure 6. SNR with eclipsing effect

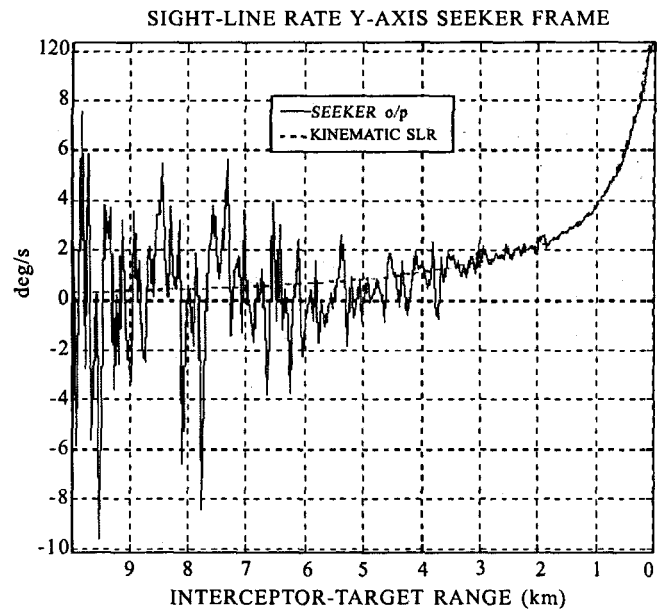


Figure 8. Sight-line rate without radar cross-section fluctuation and eclipsing effect.

range decreases<sup>4</sup>, as a function of  $1/R_{MT}$ . Figure 7 shows that when eclipsing and radar cross-section fluctuation effects are not considered, receiver angle error noise standard deviation is decreasing with interceptor-target range because SNR increases with decrease in interceptor-target range. Its effect is seen in sight-line rate output in Fig. 8. Noise content in sight-line rate decreases with interceptor-target

range appreciably. It is clear from the figure that the noise is Gaussian and it can be filtered even by a simple low pass filter. When radar cross-section fluctuation and eclipsing effect are considered, it can be seen from Fig. 9 that receiver angle error noise standard deviation fluctuates between normal (ie, without any effect) and higher value up to the maximum. The fluctuations in receiver standard

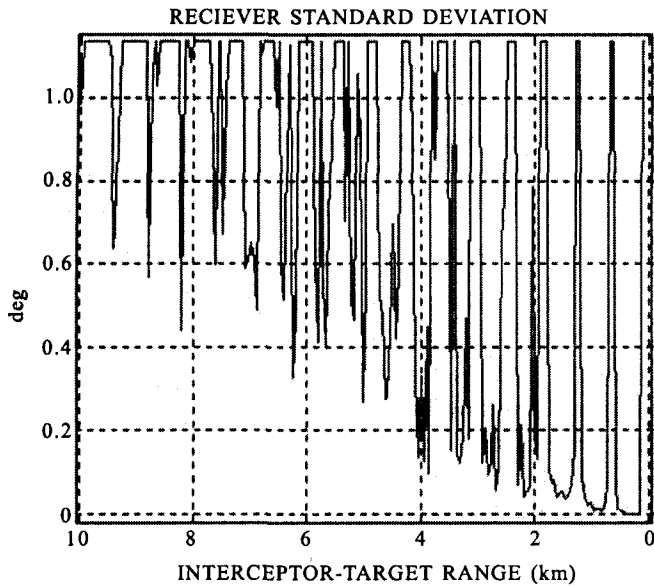


Figure 9. Receiver noise standard deviation with radar cross-section fluctuation and eclipsing effect.

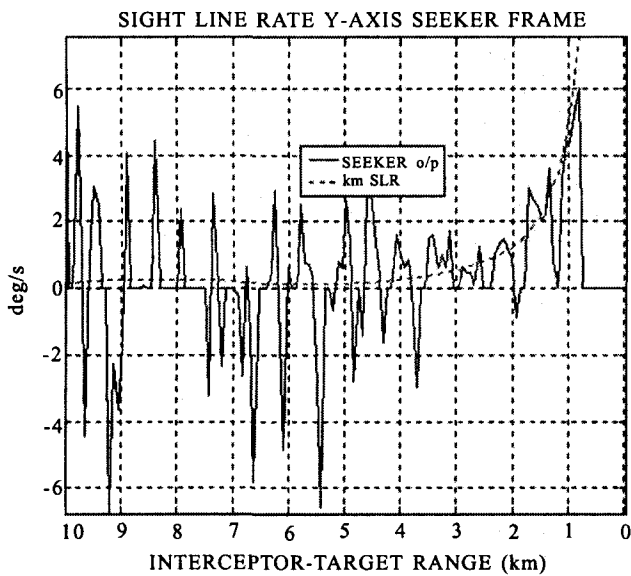


Figure 10. Sight-line rate with radar cross-section fluctuation and eclipsing effect.

deviation are appearing in measured sight-line rate (Fig. 10), which contains high level of noise even at lower interceptor-target range, and is having time-varying noise statistics.

The comparison of results of sight-line rate filtering along inertial Y-axis, with simple kinematic model (ie, three states:  $[\dot{\lambda}_{KY} \quad \ddot{\lambda}_{KY} \quad \ddot{\lambda}_{KY}]$ ) and kinematic plus three-augmented colour noise states

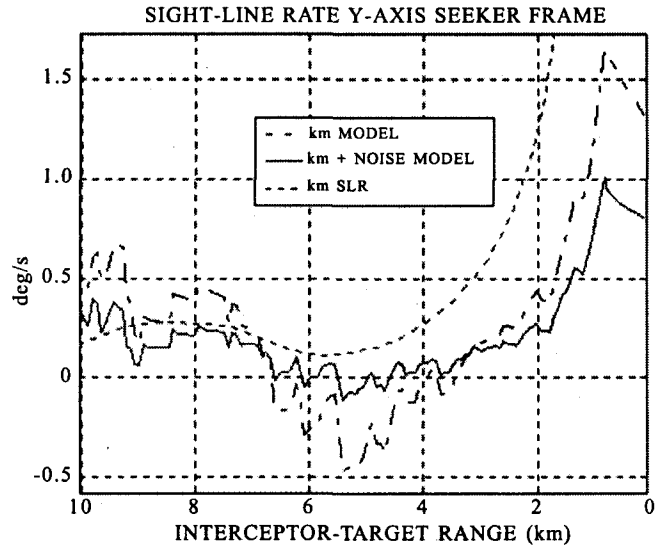


Figure 11. Comparison of performance of Kalman filter with kinematic process model and with kinematic plus noise state augmentation.

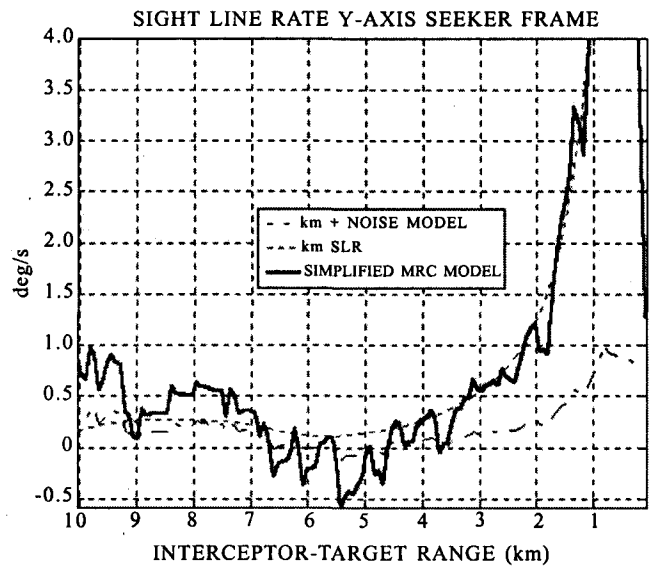


Figure-12. Comparison of performance of Kalman filter with kinematic plus noise process model and simplified MSC plus noise state process model.

model is shown in Fig. 11. It is clear from Fig. 11 that augmented model gives a better performance in terms of noise attenuation than the simple model. However, augmented model shows large lag in sight-line rate measurement at lower interceptor-target range. In the next stage, kinematic plus coloured noise state augmentation model performance is compared with the simplified model plus noise state augmentation. It can be seen from Fig. 12

that the kinematic plus noise model attenuates more noise than the simplified modified spherical coordinates (MSC) plus noise model. However, at lower interceptor-target range, kinematic plus noise model gives appreciable lag compared to the MSC plus noise model, as kinematic process model doesn't use interceptor-target dynamic information. So at lower interceptor-target ranges, it may be required to use MSC plus noise model for reasonably low estimator lag, which is essential for close-loop guidance application. For higher interceptor-target ranges, a higher-order process model and appropriate process noise variance tuning satisfy large noise attenuation requirement.

## 6. SUMMARY & FUTURE STUDY

In this study, RF seeker model is briefly highlighted and the noise in sight-line rate output of a typical RF seeker is characterised. The problem associated with filtering of colour noise in sight-line rate because of eclipsing effect and radar cross-section fluctuation is highlighted. A colour noise model has been derived and formulations of two linear Kalman filters evolved with state augmentation for coloured noise. It is shown that the augmented Kalman filter (ie, kinematic plus noise states in process model) has better noise attenuation characteristics than a simple Kalman filter. The possibility of using two different Kalman filter configurations, one at higher and the other at lower interceptor-target range is also shown. The first Kalman filter configuration gives higher noise attenuation required in the initial phase, while second Kalman filter configuration gives better sight-line rate tracking with low estimator lag required in the final stage. However, to achieve near-miss performance in close loop in the presence of latex limitation estimation, quality has to be improved further.

Further study is required to model seeker noise considering effect of body rate, glint on seeker output. Also, methods for filter lag characterisation and control are to be devised and mechanised in Kalman filter, as lag is an important parameter for guidance loop stability and miss-distance.

## ACKNOWLEDGEMENTS

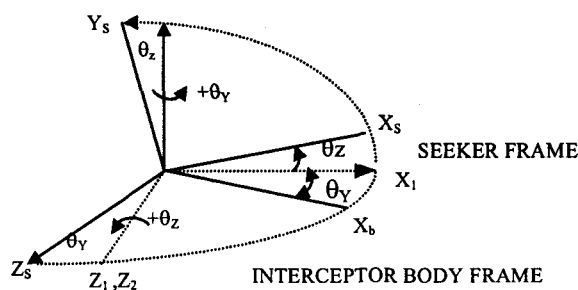
Authors take this opportunity to express their sincere gratitude to Dr V.K. Saraswat, Sarvashri Pahlada and N.V. Kadam to give opportunity to study and work on the above subject. Authors express their thanks to Wg Cdr (Retd) A.S. Sarma, Sarvashri Surendra Kumar; N. Prabhakar and his team members; and System Engineering Committee members for giving important suggestions and feedback from time to time. Authors also express their thankfulness to *Agat* Scientists and Mr R. Das and his team members for giving valuable information about seeker modelling. Authors would also like to thank Prof P.K. Nanadi and his team; Prof S. Mukhopadhyay for giving valuable information and feedback about Kalman filtering.

## REFERENCES

1. Skolnik, M. Radar Handbook, 1970.
2. Hovanessian, Radar system design and analysis. Arctect House, UK, 1984.
3. Bordon & Mumford. A stastical glint/RCS model. *IEEE Trans. Aerospace Elect. Sys.*, AES 19(5), 781-85.
4. Robinson, P.N. & Yin, M.R. Modified spherical coordinates for radar. AIAA-94-3546-CP, 55-64.

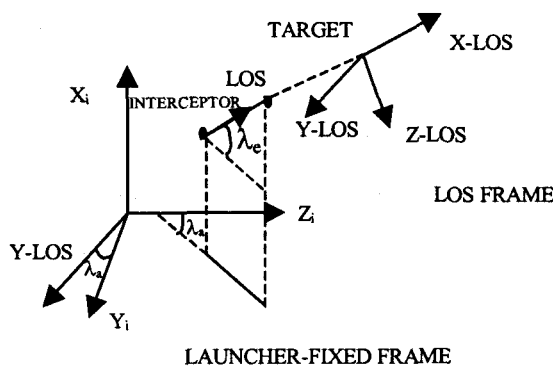
Seeker frame:

It is defined wrt interceptor body frame by two subsequent rotations; first by an angle  $\theta_y$  about body Y-axis and second by an angle  $\theta_z$  about Z-axis of newly obtained frame. With these two rotations, body longitudinal axis gets aligned with antenna axis. Using measured gimbal angles ( $\theta_{my}, \theta_{mz}$ ), interceptor longitudinal axis is aligned with the seeker antenna axis. When kinematic gimbal angles are used then longitudinal axis is aligned to true line-of-sight (line joining interceptor/seeker to target) direction. It can be seen from the figure below that the two gimbal angles are differed by boresight error.



LOS frame:

It is defined wrt launcher-fixed frame  $X_i, Y_i, Z_i$  by two rotations; first by a line-of-sight angle  $\lambda_a$  about  $X_i$  (azimuth line-of-sight angle) and then by an angle  $90 - \square_e$  ( $\square_e$  = elevation line-of-sight angle) about the newly obtained Y-axis.



Seeker frame to line-of-sight transformation can be obtained using measured gimbal angles, body attitude angles, and line-of-sight angles as follows:

$$T_{seeker2LOS} = T_{Launcher2LOS} T_{body2Launcher} T_{seeker2body}$$